

SOLUTION OF AIRFOIL-FLAP CONFIGURATIONS BY USING CHIMERA GRID SYSTEM

Erhan Tarhan, Erdal Oktay
ROKETSAN, Missile Industries, Inc., 06780 Ankara Turkey
Mehmet Ş. Kavsaoğlu
Middle East Technical University, 06531 Ankara, Turkey

Keywords: *Euler, Navier Stokes, Chimera*

Abstract

In this work, overset grid Euler/Navier-Stokes solutions of two airfoil-flap configurations and an airfoil with a deflectable flap will be presented. Overset grid systems (Chimera grids) are well-known and common technique for the solution of complex geometries and multi-body problems as well. In this study, a three-dimensional structured multi-block flow solver is modified to solve two-dimensional problems with chimera grid systems. The scheme of the flow solver is Beam-Warming with finite differencing discretization. As for the Chimera part of the code, the donor cell searching is done with ‘directional walking algorithm’ and the localization criterion is done with the ‘summation of areas’ method. For the intergrid boundary points, ‘bilinear interpolation technique’ is used. The grid points of hole regions, which are blanked out, are stored in arrays for each block in the grid-directional sense (ξ , η and ζ). The solution of matrices is carried out at each non-blanked grid patches. The required bookkeeping information is provided by a separate subprogram.

1 Introduction

As it is well known, CFD is very popular due to being cheap and once developed, easy to apply in both research and in industrial applications. However, grid dependence is one of the major problems of the CFD especially for the structured grids around the complex bodies or

bodies with multiple elements. For complex geometries or multi body configurations, either the grid generation is almost impossible or when generated the grid skewness is inevitable and the numerical errors increase.

To overcome this problem, Steger, Dougherty and Benek [9] had introduced the overset grid systems and called as ‘chimera’ the name of a mythological creature with the head of a lion, the body of a goat and the tail of a snake. They demonstrated the method by solving the Euler equations for the flow around an airfoil-flap model (SKF 1.1) and compared their results with the experimental data [10]. Later on, they presented the results of the method for three-dimensional cases [11] [12] with the steady solutions of fuselage-wing-tail configuration and fuselage with stores.

Moreover, Baysal, Fouladi and Lessard [13] applied the method for viscous solutions of three-dimensional flows around complex configurations with geometrically non-similar components. The test cases were a supersonic flow past a blunt-nose cylinder at a high angle of attack and supersonic interference flows past an ogive-nose cylinder in the close proximity of a flat plate. They compared their results with the results obtained from a single domain grid and results of the experiments. Furthermore, Terry L. Holst solved the flow around ONERA M6 wing with three-dimensional full potential equation with Chimera technique [14]. He applied a new approximate factorization within

each grid zone based on the approximate factorization scheme 2 algorithm.

Ismail H. Tuncer [4] presented a simple numerical algorithm for localizing the intergrid boundary points and for interpolation also. According to his algorithm, as the overset grid point is localized in a donor cell and automatically the weighting coefficients for the interpolation are also obtained. He claims that the algorithm is independent of numerical solution algorithms and it may easily be implemented.

In the present work, a three-dimensional structured multi-block flow solver TLNS [1] is modified to solve two-dimensional problems with chimera grid systems. The scheme of the flow solver is Beam-Warming with finite differencing discretization and it was validated with various test cases [2], [3]. The ‘directional walking’ search algorithm is applied for localization of the intergrid boundary points. For the localization criteria, ‘summation of areas’ method is used. The blanked out hole grid points are categorized for determining the array which is used for the solution of the matrices of the non-blanked grid patches in the computational directional sense (ξ , η and ζ). For these, separate subprograms are prepared. In this work, not only the problems with grids that are overset inside a solid geometry, but also problems with a solid boundary inside another solid boundary are presented.

The code is tested with the solution of two different airfoil-flap configurations (SKF 1.1 [6] and NLR7301 [7] airfoils) and an airfoil with a deflected aileron (DLBA032) [8]. The results are compared with experimental data and some references.

2 Flow Solver TLNS

The flow solver (TLNS), which is used and modified in this study, is a multi-block three-dimensional structured Euler/thin layer Navier-

Stokes solver. The scheme is Beam-Warming and finite differencing is applied. LU-ADI is used for the solution of the matrices with the use of implicit approximate factorization technique. Diagonalization procedure of Pulliam and Chaussee [15] is applied by the similarity transformations and matrix solutions reduce to scalar operations. Noting that for viscous cases, the viscous terms are neglected in the implicit operator due to the reason that the similarity transformations do not diagonalize the viscous Jacobian matrix.

$$\hat{Q}_t + \hat{E}_\xi + \hat{F}_\eta + \hat{G}_\zeta = Re^{-1} \hat{S}_\zeta \quad (1)$$

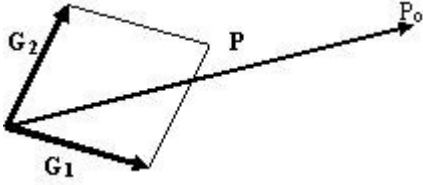
Baldwin-Lomax turbulence model is used for turbulent solutions.

The surface boundary condition is either no-slip for viscous or flow tangency for Euler solutions. The surface pressure is calculated by the normal momentum equation [16]. Extrapolation type boundary conditions are applied at the outflow boundaries. For each test case, the farfield boundary is taken at least 11 or 12 chords away.

3 Search Algorithm

In order to localize the intergrid boundary points and the other overset grid points, which are to be blanked out, several methods may be applied. Among these, Tuncer mentioned [4] the directional search algorithm and Cho, Kwon and Lee [17] presented their cut-paste algorithm for identifying the donor cells. In this work a ‘directional walking search’ algorithm is used. The reason is that the algorithm is simple to use and efficient in a way that search direction is always towards to the overset grid point. Moreover, once the overset grid point is localized, the possibility of the next one to be near the donor cell is high. In this case, within one or two iterations, the next point can be localized. In order to direct the search stencil towards the overset grid point, sign of the dot products between the relative position vector \mathbf{P} of the overset grid point and the vectors drawn

at the edges of a candidate cells (\mathbf{G}_1 , \mathbf{G}_2) are taken.



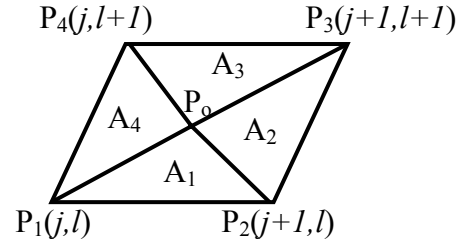
$$j = j_0 + \text{int} \left(\frac{\vec{G}_1 \cdot \vec{P}}{|\vec{G}_1 \cdot \vec{P}|} \right), l = l_0 + \text{int} \left(\frac{\vec{G}_2 \cdot \vec{P}}{|\vec{G}_2 \cdot \vec{P}|} \right) \quad (2)$$

Using above relations, the new “ j ” and “ l ”, which denote the grid point indices, are computed automatically. The search of the donor cell is initiated from an initial candidate cell. First the current cell is checked whether the overset grid point falls inside it. If it is not, after the new indices are calculated, the next candidate donor cell is checked. The procedure goes on until the back and forth movement of the search direction is detected (i.e. the indices of candidate donor cell is keep repeating) or the overset grid point is localized. If the back and forth movement is detected, the point that is being searched is either not an overset grid point and lies beyond the donor domain, or the donor grid elements in that region is highly skew and the grid elements of both domains are in incomparable sizes. This may result in that although the search stencil changes direction, the point is never localized. This is the main problem of this search algorithm. To overcome this problem, an interval of “ Δj ” and “ Δl ” indices, say 5 or 10, is given and a region of $(j-\Delta j, j+\Delta j)$, $(l-\Delta l, l+\Delta l)$ is specified. Then the point is searched in this region.

4 Localization Criteria

In this work, in order to check whether the searched grid point falls inside the candidate donor cell (P_1, P_2, P_3, P_4), the ‘summation of areas’ method is applied. According to the algorithm, the summation of the triangular areas

formed by the 4 corners of the cell and the point to be localized must be equal to the area of the cell itself.



$$\sum A_{1234} \cong \sum_{i=1,4} A_i \quad (3)$$

Since the numerical calculation leads to some precision loss, near-equal sign is used in above equation. The ratio of the calculated areas is compared with 1.0. An accuracy parameter, ε , is used for this purpose. $\varepsilon = 10^{-4}$ is used in this study. The reason for comparing the area ratio, instead of the difference in areas, is that in Navier Stokes type grids some areas may be less than ε .

$$\text{abs} \left[1.0 - \frac{\sum_{i=1,4} A_i}{\sum A_{1234}} \right] \leq \varepsilon \quad (4)$$

Area of a triangle can be calculated as in the following;

$$A = 0.5 |\vec{E}_1 \times \vec{E}_2| \quad (5)$$

In above equation, \mathbf{E}_1 and \mathbf{E}_2 denote the vectors drawn at the two edges of the triangle. Blanked out grid points of NLR7301 airfoil with a trailing edge flap and DLBA032 airfoil with its deflected flap are shown in the Figures 1 and 2.

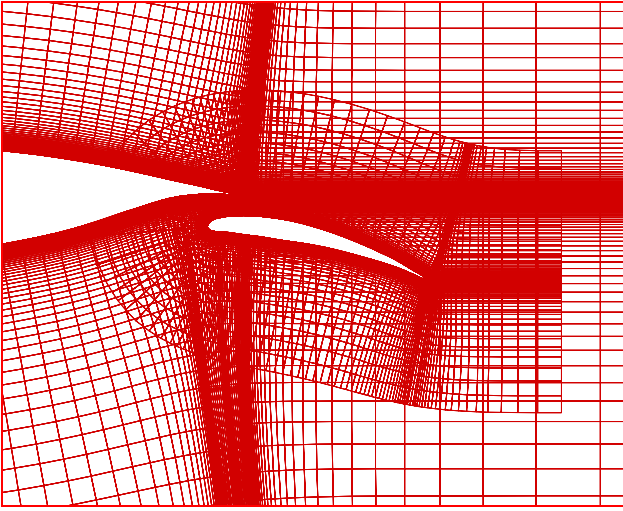


Fig. 1 Grids of NLR7301 airfoil with trailing edge flap.

5 Modification of the Flow Solver

In order to modify the flow solver to implement the chimera, two major features are considered: the implementation of the bilinear interpolation and modification of the matrix solutions.

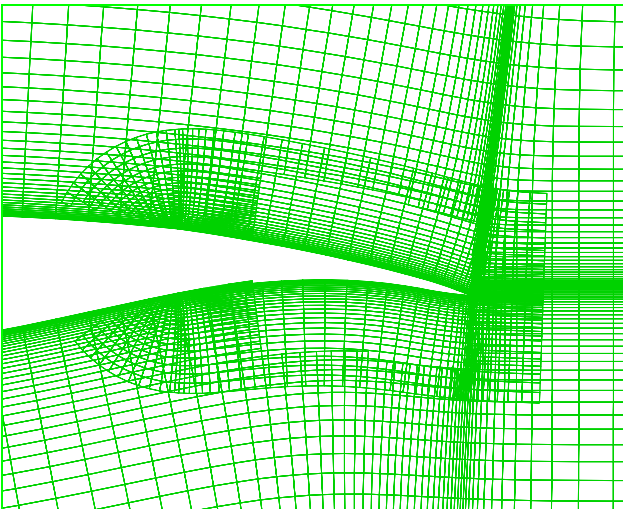


Fig. 2 Grids of DLBA032 airfoil with deflectable flap ($\delta_{\text{defl}}=2.0$ Deg).

To modify the implicit operations on the flux Jacobians, the non-blanked patch information is stored via a separate bookkeeping subprogram. With the program each domain is investigated

through the (ξ, η, ζ) directions to check at which index stations does the blanked-out region start and end. Also the number of blanked-out patches along the direction is kept in another array. With this bookkeeping procedure, IBLANK array is not inserted in to the matrix solutions as a coefficient. Besides the computational work is lessened.

6 Interpolation

Before the time marching iteration starts, the interpolation boundary conditions are applied to the intergrid boundary points. The interpolation model used is the *bilinear interpolation*. According to Mastin and McConnaughey [18], bilinear interpolation is superior to the Taylor Series expansion since the higher order derivatives are also included. They claim that, when the two overlap grid elements are in comparable lengths, two-cell overlapping for the interpolation is enough.

According to the interpolation technique, any given quadrilateral donor cell is converted to a unit square for which the following iso-parametric equation of the face can be written;

$$\varphi = d_1 + d_2\xi + d_3\zeta + d_4\xi\zeta \quad (6)$$

In the above equation the coefficients ' d_i ' are determined using the Cartesian coordinates of the cell corners. The aim is to determine the (ξ, ζ) values of the Cartesian coordinates of the overset grid point when it is defined as in the iso-parametric form. Once they are determined, the flow variable of the overset point can easily be interpolated using the iso-parametric form. The detailed description of the method for three-dimensional case is presented in [5].

7 Test Cases

The flow solver is tested for the chimera applications with various two-dimensional test cases. Among these, two different airfoils with maneuvering flap configurations and an airfoil

with deflectable aileron geometry are presented in this work.

7.1 SKF 1.1 Airfoil-Flap Configuration

The first test case is a supercritical airfoil (SKF 1.1) with maneuver flap geometry. The experiments were carried at ONERA S3 Modane and DFVLR wind tunnels. The freestream conditions selected for the flow solutions are $M_\infty=0.7$, the angle of attack $\alpha_g=3.0$ Deg and $Re \approx 2.3$ million with free transition. The 5th configuration of reference [6] is selected as the test geometry. In this configuration, the gap between the airfoil and the flap is 1.55 % of the chord of the airfoil. The flap deflection angle is 10 Deg.

On the airfoil geometry, some modifications are done for convenience in computations. On the original geometry, there is a cavity through the airfoil when the flap is apart where the corners are sharp. Moreover, again in the original geometry, the trailing edge of the airfoil is truncated and therefore it is not pointed. Modelling the geometry with its original description was leading the flow separation and vortex formation inside the cavity and hence blocking the flow passage inside the gap at transonic speeds. In order to enlarge the cavity entrance and ease the flow through the gap, the cavity corner is smoothed and the trailing edge thickness is decreased to zero.

As for the grid topology, two C type structured grid domains are generated around the airfoil and flap. The grid dimensions are 361x87 for the airfoil with 297 grid points along the airfoil surface and 180x51 for the flap geometry whose 160 points define the flap geometry. Euler and Navier Stokes with turbulent flow solutions are made for this case. Baldwin-Lomax algebraic model is used for the turbulence. The geometry and grids are in Fig. 3 and Fig. 4.

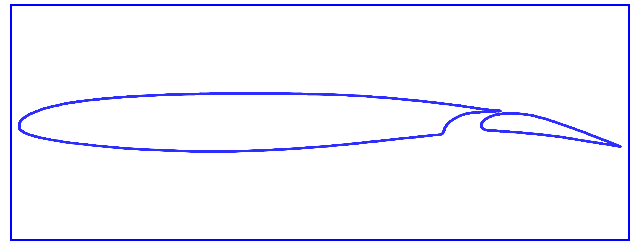


Fig. 3 SKF 1.1, supercritical airfoil geometry with a maneuver flap.

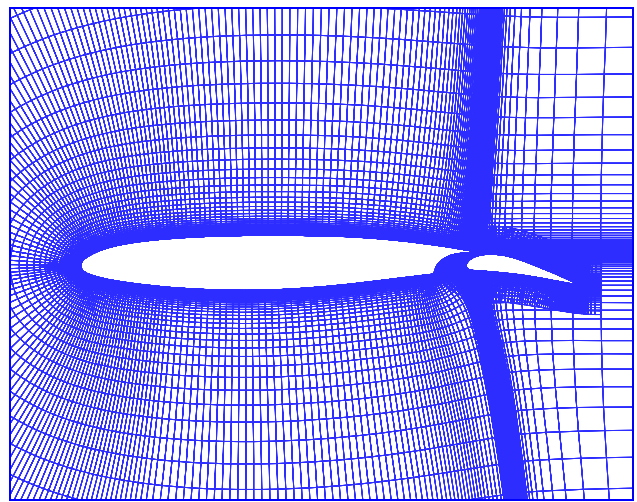


Fig. 4 SKF 1.1 mesh view with blanked out regions.

7.2 NLR7301 Airfoil Section with a Trailing Edge Flap

The second test case is composed of again an airfoil section with a trailing edge flap, namely NLR7301 airfoil with flap geometry. The wind tunnel tests were carried at NLR LST tunnels. The test data were so designed that nowhere but around small region of wing nose, flow separation occurs. The 32% chord trailing edge flap is deflected 20 deg. For the current configuration, the gap distance is 2.6% chord and overlap length is 5.3% chord [7]. The freestream is $M_\infty=0.185$ and the angle of attack is $\alpha=6.0$ deg. Reynolds Number is taken as $Re_c=2.51$ million.

As for the grid topology, again two separate C type grid domains are generated around the airfoil. The grid dimensions for Euler solutions are 223x63 with 159 grid points defining the airfoil geometry and 128x28 with 110 grid points defining the flap geometry. On the other hand, for the viscous solutions, 239x123 points for the airfoil grid and 150x58 points for the flap geometry are generated. For the viscous grids initial grid spacing is taken as $dz_0 \approx 1.0 \times 10^{-5}$. In the following figures the airfoil-flap geometry and the chimera grids can be seen (Figures 5, 6).

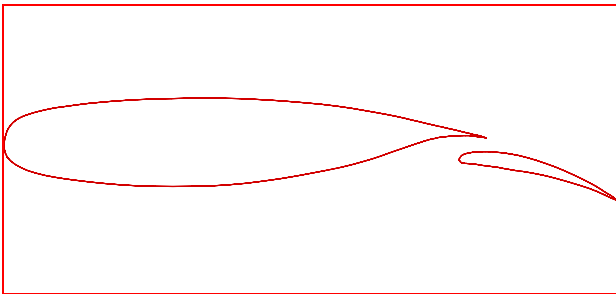


Fig. 4 NLR7301 airfoil with a trailing edge flap.

7.3 DLBA032 Airfoil With Deflectable Aileron

The last case solved by the use of chimera grids is DLBA032 – a supercritical airfoil - with deflecting aileron. The experimental data were obtained from IAR High Reynolds Number Two-Dimensional Test Facility.

The dominant flow physics are the shock development and trailing edge separation. In the experimental data the deflection angles are ranging from -5 to $+5$ deg. The aileron hinge is located at 75% chord of the airfoil. For the current test conditions fixed transition is used according to the experimental procedure. The freestream Mach is around $M_\infty=0.730$, the angle of attack is around $\alpha=2.771$ and the $Re \approx 5$ million. The freestream conditions may change from one case to another for different deflection angles.

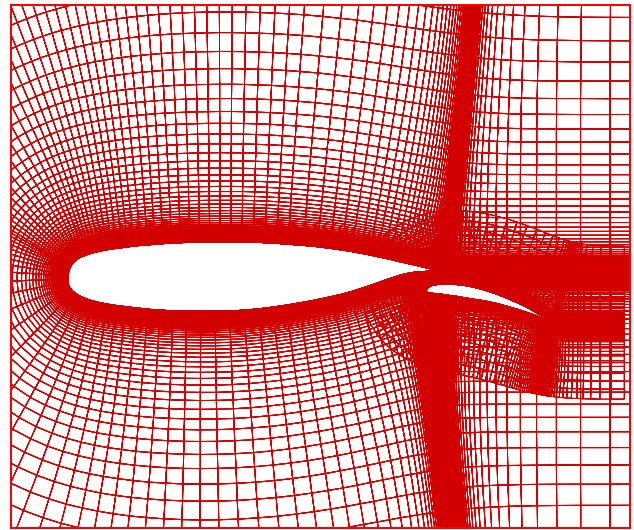


Fig. 5 Mesh view of NLR7301 airfoil-flap with the blanked out regions.

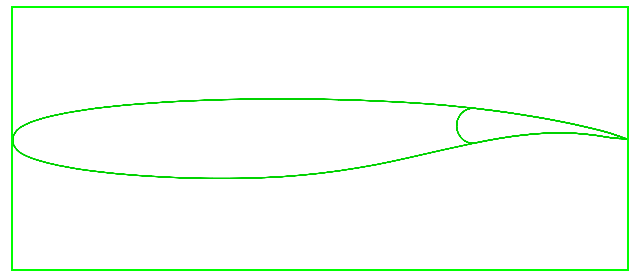


Fig. 6 DLBA032 airfoil-deflectable flap geometry.

Before proceeding with chimera applications for this test case, the single block TLNS runs are performed in order to see the discrepancies between the single block runs, experiment and chimera runs.

Another feature of the test case is that, the chimera grid domains merge into each other in order to define the airfoil-flap geometry correctly. Not only the interior points, but also solid boundary points of a domain fall inside the other solid geometry.

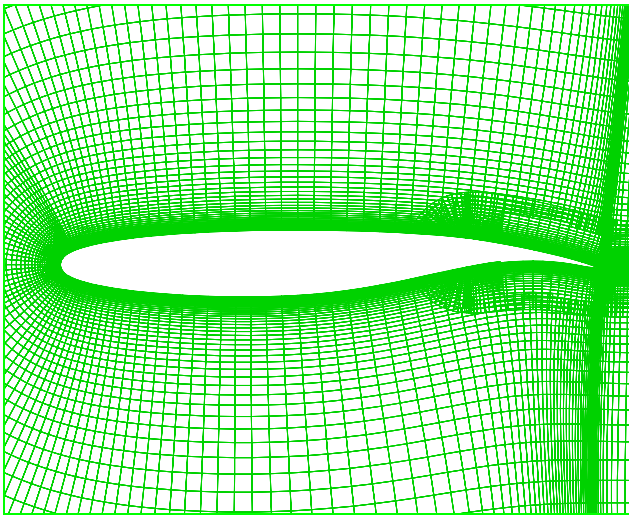


Fig. 7 DLBA032 airfoil with deflected flap ($\delta_{\text{defl}}=2.0$ deg.).

For chimera applications typically the similar grids are used: Two separate grid domains for the base airfoil and aileron geometry as shown in Figure 7. The grid dimensions for the Euler chimera solutions are 223×73 points for the base airfoil (with 167 points along the surface) and 121×26 points for the aileron (with 97 points along the surface). For the single block cases, for each deflection angle, a new mesh is generated. The typical adapted grid dimensions for viscous and Euler computations are 247×121 and 247×73 having 189 points along the surface.

8 Results

The Navier-Stokes solution of the first test case (SKF 1.1 airfoil with maneuver flap) is shown in the Figure 8 with the Mach contours around the geometry. There is a flow separation at the corner of the cavity and due to that, a vortex formation is seen inside the cavity (Figure 9). Since the vortex formation blocks the passage of the gap and due to viscous effects, the suction pressure over the flap is not correctly predicted when compared with the experimental results (Figure 10). On the other side, the Euler solution of the flow shows better C_p values over the flap comparing with the turbulent results. For the Euler solutions, since the suction

pressure over the flap is affected by the shock formation at the trailing edge of the airfoil, it is underpredicted. In either case the C_p values are overpredicted over the airfoil when compared with the experimental results. Shock formation is better located when the Navier Stokes with turbulent solution is performed. However, due to that the grid is not flow-adapted, shock formation can not be clearly seen in the Figure 10. The current chimera results are in agreement with the results of Benek et al.

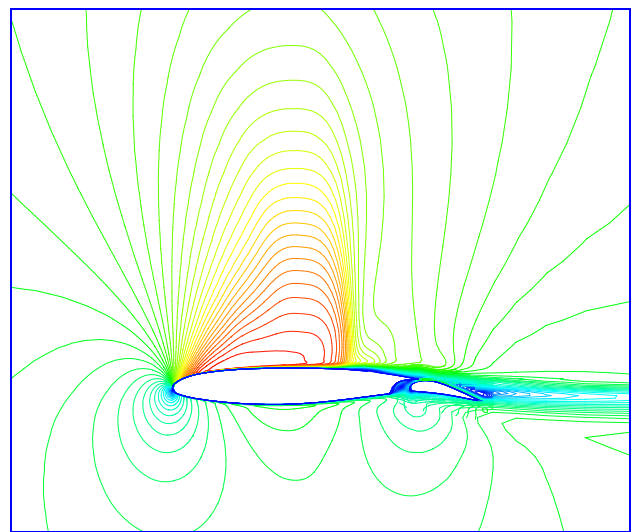


Fig. 8 Mach contours around the SKF 1.1 airfoil-flap geometry.

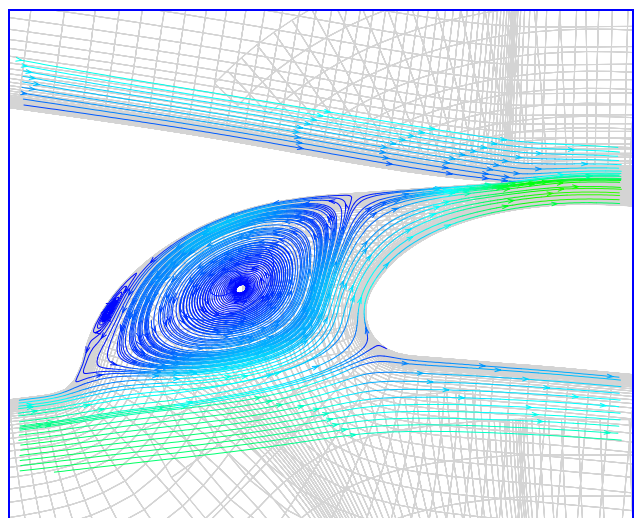


Fig. 9 Streamlines inside the cavity and the gap of SKF 1.1.

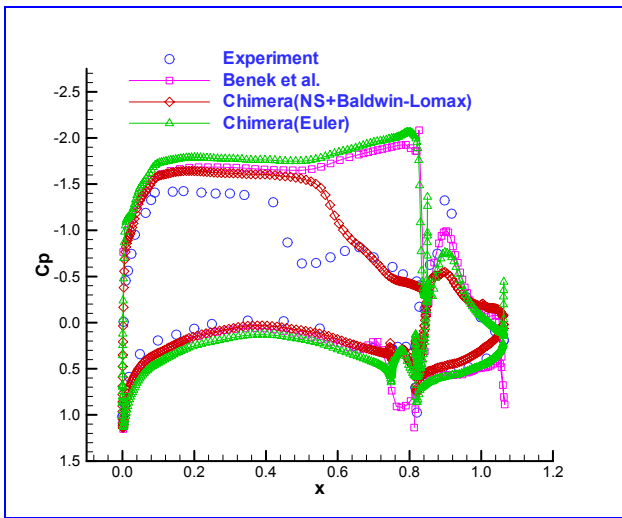


Fig. 10 SKF 1.1 pressure coefficients.

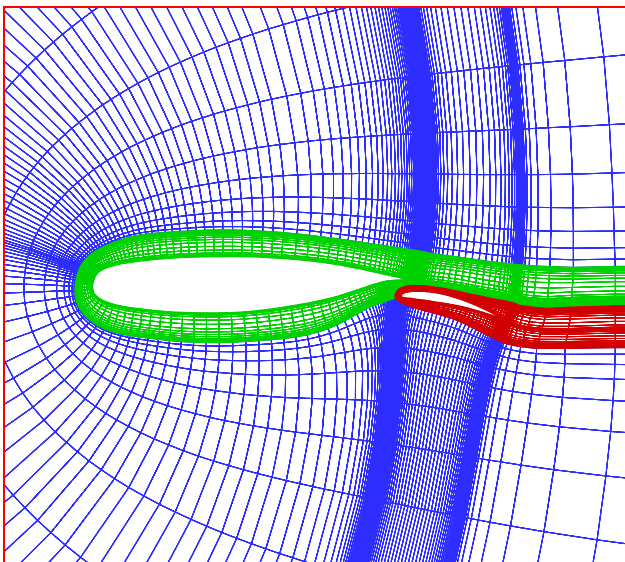


Fig. 11 Multi-block grid of the NLR7301 airfoil and the trailing edge flap geometry.

For the second test case (NLR7301 airfoil with trailing edge flap), both chimera and multi-block solutions are obtained. The grid structure of the multi-block solution is shown in Figure 11 which can be compared with the chimera grid shown in Figure 5. Both Chimera and multi-block solutions of TLNS show agreement with the experimental result. In fact, for this case the freestream Mach number is very low, i.e. $M_\infty=0.185$ for a compressible flow solver. In Figures 12 and 13, Mach contours around the

airfoil-flap geometry and pressure coefficient values are presented.

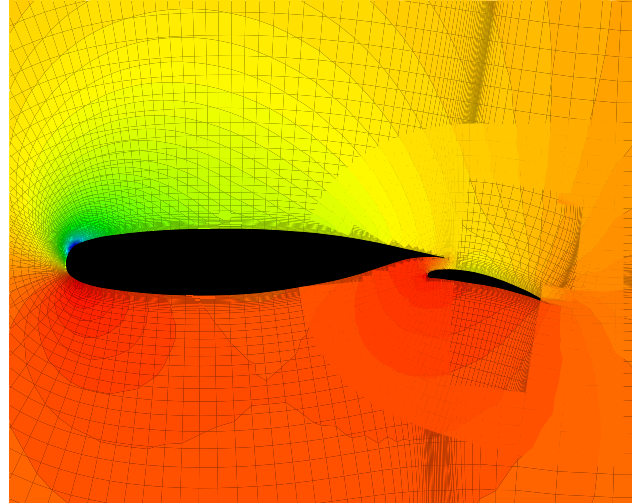


Fig. 12 Mach contours around the NLR7301 airfoil and trailing edge flap geometry.

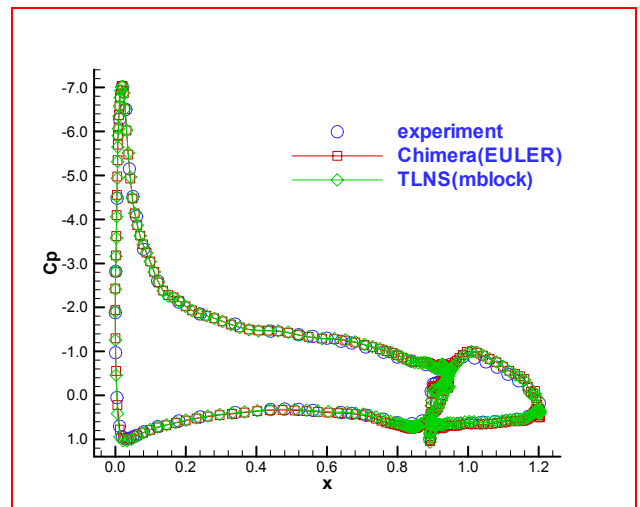


Fig. 13 NLR7301 pressure coefficients.

For the last test case (DLBA032 airfoil with deflectable aileron), both chimera and single block Euler solutions show good agreement with the experimental results in forebody pressure magnitudes (Figures 14,15). On the other hand, Euler solutions can not predict shock location correctly as expected. The discrepancy between the TLNS (Euler) and Chimera (Euler) solutions around the shock location is due to the difference in grid

topologies and densities. Turbulent single block Navier Stokes solution of the flow underpredicts the pressure values both in the suction and pressure sides (Figure 14), although the shock location and the flow separation at the trailing edge are correctly predicted. For the Chimera Euler solution, Mach contours around the airfoil-aileron are shown in Figure 16.

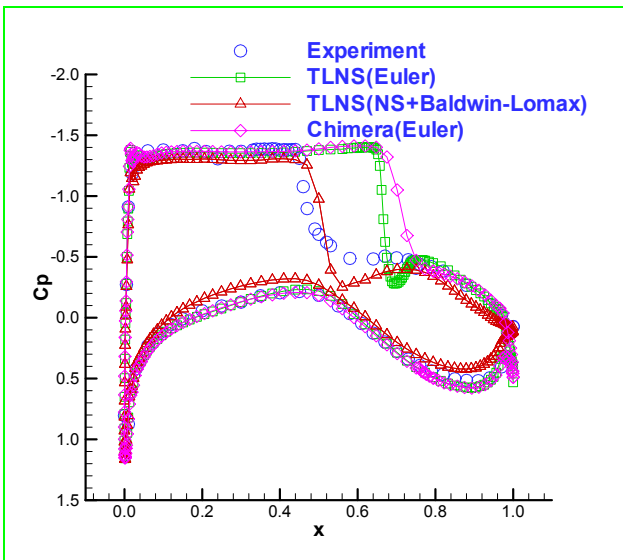


Fig. 14 DLBA032 pressure Coefficients ($\delta_{defl}=0.0$ deg).

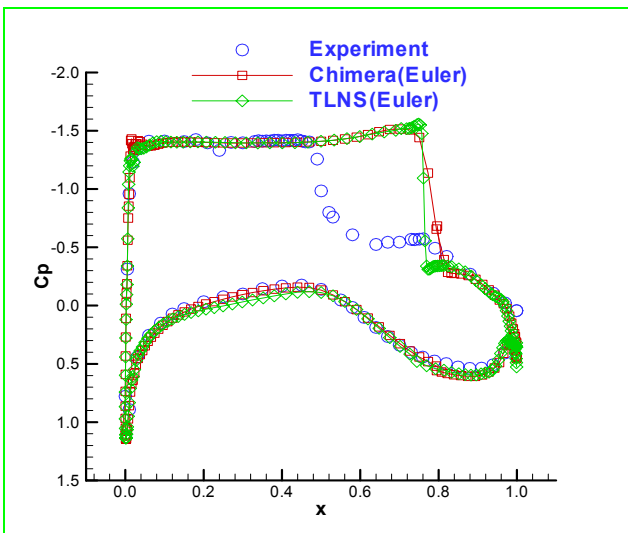


Fig. 15 DLBA032 pressure coefficients ($\delta_{defl}=2.0$ deg).

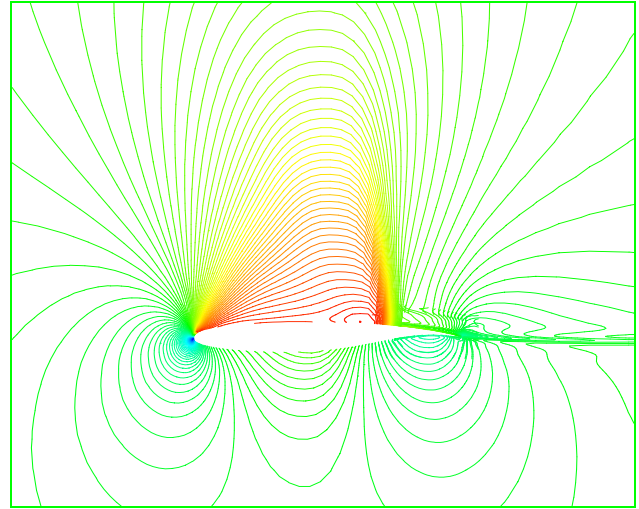


Fig.16 Mach contours around DLBA032 airfoil with $\delta_{defl}=2.0$ deg, Chimera-Euler solution.

Discussion and Conclusion

In this work, both chimera, single and multi-block solutions are presented and compared. The solutions are performed with either Euler or Navier Stokes equations with Baldwin Lomax turbulence model. The results may show some discrepancies when compared with the experimental results. However, the chimera grid solutions produce similar results with the references and same results with the single or multi-block solutions if the grid qualities are similar. There may be some discontinuities across the intergrid boundaries. The reasons are due to that the interpolation methods, even they may be accurate, are non-conservative and also grid topologies and sizes are different in those regions. On the other hand, chimera is a powerful method in that grid generation is easier and when the geometry definitions change, another mesh generation is not required.

For practical applications, it is concluded that the results obtained with the Chimera grids are acceptable.

References

- [1] Oktay E, Alemdaroğlu N, Tarhan E, Chamigny P, d’Espiney P. Euler and Navier-Stokes Solutions for Missiles at High Angles of Attack. *Journal of Spacecraft and Rockets*, Vol. 36, No. 6, pp. 850-858, November-December 1999.
- [2] Pulliam T H and Barton J T. Euler Computations of AGARD Working Group 07 Airfoil Test Cases. AIAA-85-0018, 1985.
- [3] Kaynak Ü. Advances in the Computation of Transonic Separated Flows over Finite Wings. AIAA-87-1195, 1987.
- [4] Tuncer I H. Two-Dimensional Unsteady Navier-Stokes Solution Method with Moving Overset Grids. *AIAA Journal*, Vol. 35, No. 3, pp. 471-476, 1997.
- [5] Benek J A, Steger J L, Dougherty F C and Buning P G. Chimera: A Grid-Embedding Technique. AEDC-TR-85-64 (AD-A167466), April 1986.
- [6] Stanewsky E, Thibert J J. Airfoil SKF 1.1 With Maneuver Flap. *Experimental Data Base For Computer Program Assessment*. AGARD AR-138, pp. A5-1 – A5-29, May 1979.
- [7] Van den Berg B and Gooden J H M. Low Speed Surface Pressure and Boundary Layer Measurement Data For The NLR7301 Airfoil Section With Trailing Edge Flap. AGARD-AR-303 Vol. 2, pp. A9-1 – A9-12, 1994.
- [8] Chin V D, Dominik C J, Lynch F T and Rodriguez D L. 2-D Aileron Effectiveness Study. AGARD-AR-303 Vol. 2, pp. A5-1 - A5-20, 1994.
- [9] Steger J L, Dougherty F C and Benek J A. A Chimera Grid Scheme. *Advances in Grid Generation*, ASME FED-5 American Society of Mechanical Engineers, pp. 59-69 New York, 1983.
- [10] Benek J A, Steger J L and Dougherty F C. A Flexible Grid Embedding Technique With Application to the Euler Equations. AIAA-83-1944, July 1983.
- [11] Benek J A, Buning P G and Steger J L. A 3-D Chimera Grid Embedding Technique. AIAA-85-1523, July 1985.
- [12] Dougherty F C, Benek J A and Steger J L. On Applications of Chimera Grid Schemes To Store Separation. NASA TM-88193, October 1985.
- [13] Baysal O, Fouladi K and Lessard V. R. Multigrid and Upwind Viscous Flow Solver on Three-Dimensional Overlapped and Embedded Grids. *AIAA Journal*, Vol. 29, No. 6, pp. 903-910, 1991.
- [14] Holst T L. Multizone Chimera Algorithm for Solving the Full-Potential Equation. *Journal of Aircraft*, Vol. 35, No. 3, pp. 412-421, 1998.
- [15] Pulliam T H and Chaussee D S. A Diagonal Form of an Implicit Approximate Factorization Algorithm. *Journal of Computational Physics*, Vol. 39, pp. 347-363, 1981.
- [16] Pulliam T H and Steger J L, Recent Improvements in Efficiency, Accuracy and Convergence for Implicit Approximate Factorization Algorithms. AIAA- 85-0360, 1985.
- [17] Cho K W, Kwon J H, Lee S. Development of a Fully Systemized Chimera Methodology for Steady/Unsteady Problems. *Journal of Aircraft*, Vol. 36, No. 6, pp. 973-980, November-December 1999.
- [18] Mastin C W and McConnaughey H V. Computational Problems on Composite Grids. AIAA-84-1611, 1984.